Nanoscale Res Lett (2010) 5:512–517
DOI 10.1007/s11671-009-9518-0

SPECIAL ISSUE ARTICLE

Composite Electrodes for Electrochemical Supercapacitors

Jun Li · Quan Min Yang · Igor Zhitomirsky

Received: 30 July 2009 / Accepted: 17 December 2009 / Published online: 7 January 2010
© The Author(s) 2010. This article is published with open access at Springerlink.com

Abstract Manganese dioxide nanofibers with length ranged from 0.1 to 1 μm and a diameter of about 4–6 nm were prepared by a chemical precipitation method. Composite electrodes for electrochemical supercapacitors were fabricated by impregnation of the manganese dioxide nanofibers and multiwalled carbon nanotubes (MWCNT) into porous Ni plaque current collectors. Obtained composite electrodes, containing 85% of manganese dioxide and 15 mass% of MWCNT, as a conductive additive, with total mass loading of 7–15 mg cm^{-2}, showed a capacitive behavior in 0.5-M Na_2SO_4 solutions. The decrease in stirring time during precipitation of the nanofibers resulted in reduced agglomeration and higher specific capacitance (SC). The highest SC of 185 F g^{-1} was obtained at a scan rate of 2 mV s^{-1} for mass loading of 7 mg cm^{-2}. The SC decreased with increasing scan rate and increasing electrode mass.

Keywords Manganese dioxide · Carbon nanotube · Nickel plaque · Supercapacitor · Impregnation · Composite

Introduction

Porous Ni materials, such as plaques [1] and foams [2], are widely used in industry for the fabrication of electrodes for rechargeable batteries. Nanostructured active materials are impregnated chemically or electrochemically into the porous Ni structures, which are used as current collectors [3]. Ni plaques are current collectors of choice for battery applications demanding high power and reliability, along with long cycle life, such as batteries for aerospace and railway applications, power tools and some portable electronics [1]. The pore size of Ni plaques is smaller compared to that of foams. The smaller pore size decreases the distance for electrons to travel from the current collector into the active material during cell discharge and consequently improves the discharge rate characteristics for high power applications [3]. Significant advances in the development of Ni plaques were achieved by the use of filamentary Ni particles with high surface area, which improved contact with active materials [4].

A new wave of interest in the application of porous Ni materials is related to the development of electrochemical supercapacitors (ES) [5]. ES can complement or replace batteries in electrical energy storage applications when high-power delivery is required [6]. Manganese dioxides with various crystalline structures are important materials for electrodes of ES [7]. The interest in the application of manganese dioxide in ES is related to low cost of this material, which exhibits high SC in environmentally friendly aqueous electrolytes [8].

The charging mechanism of manganese dioxide electrodes of ES is described by the following reaction [9]:

$$MnO_2 + A^+ + e^- \leftrightarrow MnO_2A \quad (1)$$

where $A^+ = Li^+, Na^+, K^+, H^+$. Equation 1 indicates that high electronic and ionic conductivity of the electrode material are important in order to utilize the high theoretical capacitance (1,370 F g^{-1}) of manganese dioxide [10]. Composite [11] and thin film electrodes [12] were developed and investigated. The properties of MnO_2 are influenced by

J. Li · I. Zhitomirsky (✉)
Department of Materials Science and Engineering, McMaster University, 1280 Main Street West, Hamilton, ON L8S 4L7, Canada
e-mail: zhitom@mcmaster.ca

Q. M. Yang
Vale Inco Limited, Mississauga, ON L5K 1Z9, Canada

crystalline structure, particle size, porosity and surface area [13]. A complicating factor in the application of MnO_2 in ES is low electronic conductivity of this material. This problem can be addressed by the use of advanced current collectors, such as Ni plaques.

In a previous investigation [14], manganese dioxide nanofibers were prepared by a chemical precipitation method and utilized for the fabrication of composite manganese dioxide—MWCNT films by electrophoretic deposition. The composite films deposited on stainless steel foils showed high SC in a voltage window of 1.0 V. However, the SC decreased significantly with increasing film thickness. The results presented below indicated that relatively high SC can be achieved at high active material loading using Ni plaques as current collectors. In this approach, the high surface area and porous structure of the Ni plaques provided improved electrical contact of the current collector with active material and enabled good electrolyte access to the active material. We presented experimental results on the fabrication of composite electrodes, investigation into electrode microstructure and electrochemical behavior.

Experimental Procedures

Manganese dioxide nanofibers were prepared by the method described in the previous investigation [14]. In this approach, precipitation was performed by the reduction of 0.2-M $KMnO_4$ (Aldrich) solutions with ethanol using the following reaction:

$$4MnO_4^- + 3\ CH_3CH_2OH + 4H^+ \rightarrow 4MnO_2 + 3\ CH_3COOH + 5\ H_2O \quad (2)$$

MWCNT were provided by Arkema company. The average diameter of MWCNT was ~15 nm and length ~0.5 μm. Ni plaques with mass of 0.1 mg cm^{-2} were provided by Inco company and impregnated with a manganese dioxide slurry containing 15 mass% of MWCNT.

XRD studies were performed with a diffractometer (Nicolet I2) using monochromatic Cu Kα radiation at a scanning speed of 0.5 deg min^{-1}. TGA and DTA of the manganese dioxide nanofibers were carried out in air at a heating rate of 5 °C/min using a thermoanalyzer (Netzsch STA-409). Electron microscopy investigations were performed using a JEOL 2010F transmission electron microscope and a JEOL JSM-7000F scanning electron microscope equipped with energy-dispersive spectroscopy.

Capacitive behavior of the electrodes was studied using a potentiostat (PARSTAT 2273, Princeton Applied Research) controlled by a computer using a PowerSuite electrochemical software. Electrochemical studies were performed using a standard three-electrode cell containing 0.5 M-Na_2SO_4 aqueous solution degassed with purified nitrogen gas. The surface area of the working electrodes was 1 cm^2. The counter electrode was a platinum gauze, and the reference electrode was a standard calomel electrode (SCE). Cyclic voltammetry (CV) studies were performed within a potential range of 0–1.0 V versus SCE at scan rates of 2–100 mV s^{-1}. The SC was calculated using half the integrated area of the CV curve to obtain the charge (Q), and subsequently dividing the charge by the mass of the active material (m) and the width of the potential window (ΔV):

$$C = Q/m\Delta V \quad (3)$$

Impedance spectroscopy investigations were performed in the frequency range of 0.1 Hz–100 kHz at amplitude voltage of 5 mV. Simulations of the impedance behavior were performed on the basis of the equivalent-circuit models using ZsimpWin 3.10 commercial software.

Results and Discussion

In the previous investigation [14], manganese dioxide nanofibers were prepared by the reduction in $KMnO_4$ solutions with ethanol, followed by stirring of obtained suspensions during 20 h, and then washing and drying of the suspension. As an extension of the previous investigation, the stirring time was varied in the range of 1–20 h. Figure 1a, b show typical TEM images of the nanofibers obtained after 1 h of stirring. The diameter of the nanofibers was 4–6 nm and length 0.1–1 μm. It was found that the nanofibers were not individual crystals but were composed of small nanoparticles with typical size less than 5 nm. The diameter of the nanofibers was non-uniform (Fig. 1b). The increase in the stirring time from 1 to 20 h resulted in partial agglomeration of the nanofibers, which formed bundles (Fig. 1c), containing individual nanofibers. This result was in a good agreement with the results of investigation into other nanomaterials [15], which indicated that stirring of nanoparticles can promote agglomeration.

XRD studies (Fig. 2) showed changes in the diffraction patterns of the nanofibers with increasing stirring time. The XRD pattern of the nanofibers stirred for 1 h showed XRD peaks of birnessite, corresponding to the JCPDS file 87-1497. According to the literature, birnessite has a two-dimensional layered structure that consists of edge-shared MnO_6 octahedra with cation and water molecules occupying the interlayer regions [16]. The birnessite formula is generally expressed as $A_xMnO_{2+y}(H_2O)_z$, in which A represents an alkali metal cation. The average oxidation state of Mn usually falls between 3.6 and 3.8, which represents a predominance of Mn^{4+} with minor amounts of Mn^{3+} and Mn^{2+} [16]. The intensity of the peaks of the birnessite phase

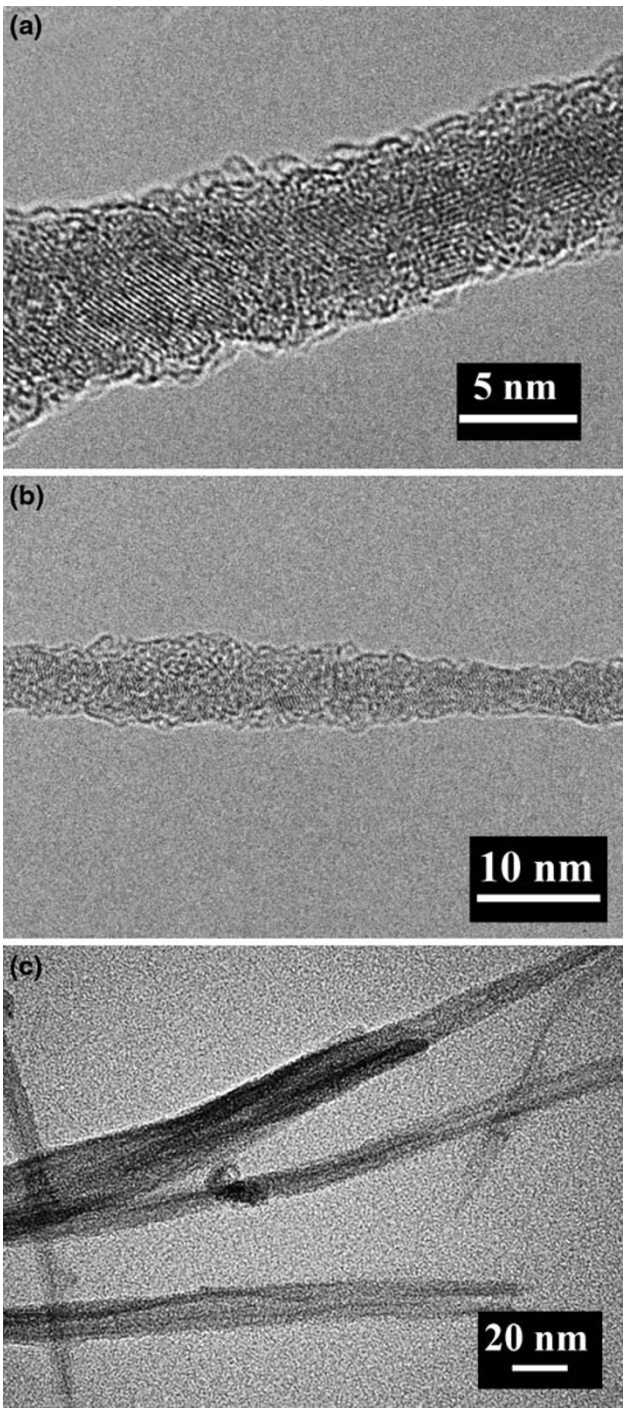

Fig. 1 TEM images of the nanofibers **a**, **b** after stirring during 1 h and **c** typical bundles formed after stirring during 20 h

decreased with increasing stirring time, indicating lower crystallinity. After 20 h of stirring, the XRD pattern showed very small broad peaks. It was suggested that the nanofibers contained crystalline and amorphous phases.

It was found that the precipitated manganese dioxide nanofibers contained potassium and adsorbed water. EDS studies showed the K/Mn atomic ratio of 0.16 ± 0.03 and

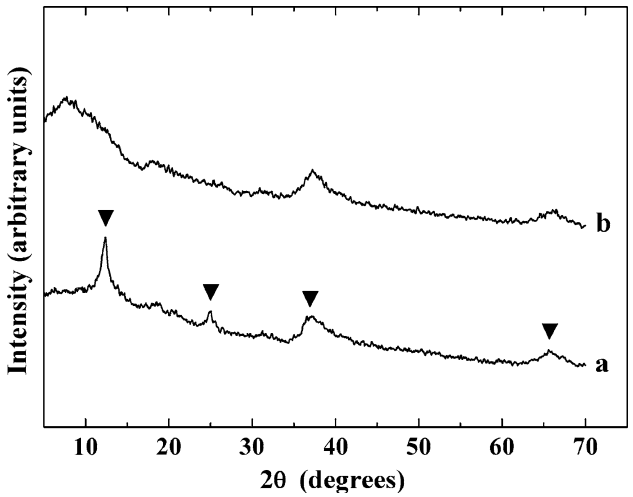

Fig. 2 X-ray diffraction patterns for powders, containing nanofibers stirred during **a** 1 and **b** 20 h (*inverted filled triangle*—JCPDS file 87-1497)

0.14 ± 0.03 for nanofibers stirred during 1 and 20 h, respectively. Figure 3 shows TGA and DTA data for the nanofibers stirred during 1 h. The TGA studies of the powders showed the mass loss related to the dehydration at temperatures below 400 °C. Corresponding DTA data showed a broad endotherm at ~150 °C. Small mass gain in the range of 400–420 °C in TGA data and corresponding DTA exothermic peak can be attributed to oxidation of non-stoichiometric manganese dioxide. The mass loss in the range of 880–900 °C and corresponding endotherm can be attributed to reduction of manganese dioxide in agreement with the literature data [17]. Similar behavior was observed for the nanofibers stirred during 20 h.

The slurries containing manganese dioxide nanofibers and MWCNT were used for the impregnation of Ni plaques. Figure 4a shows a schematic of the cross-section of a

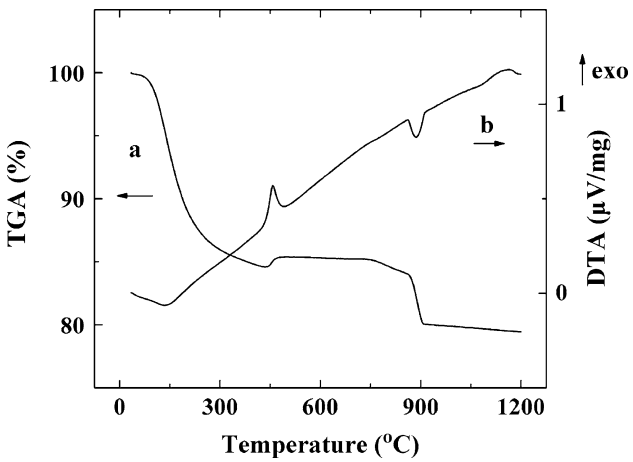

Fig. 3 **a** TGA and **b** DTA data for nanofibers stirred during 1 h (*exo*—shows exothermic effects)

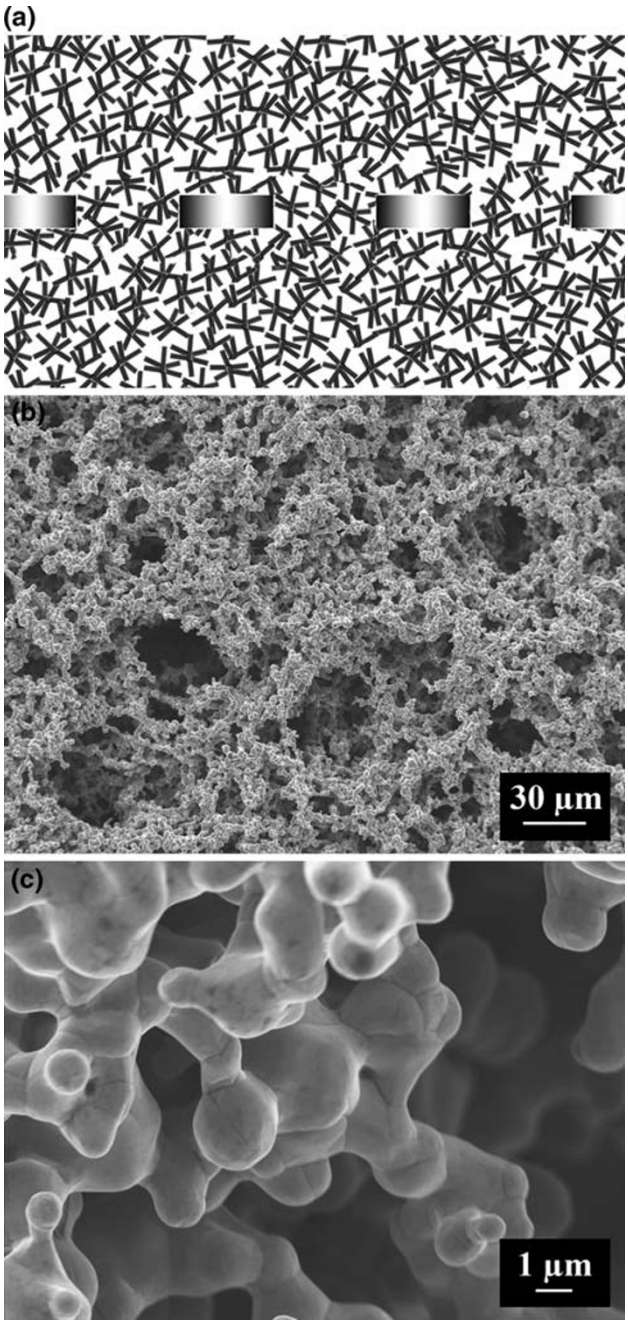

Fig. 4 **a** Schematic of a cross-section of a Ni plaque, containing perforated Ni foil (thickness 0.1 mm) and sintered Ni particles (1–3 µm) and **b**, **c** SEM images of the surface of a Ni plaque at different magnifications

Ni plaque, which consists of a perforated Ni foil and sintered Ni particles. The voids between the particles provide a space for the loading of the plaques with an active material. Figure 4b, c show SEM images of the surface of a Ni plaque at different magnifications. The plaques exhibited porous microstructure with pore size in the range of 1–50 µm (Fig. 4b). The SEM image obtained at higher magnification (Fig. 4c) showed small particle size of Ni

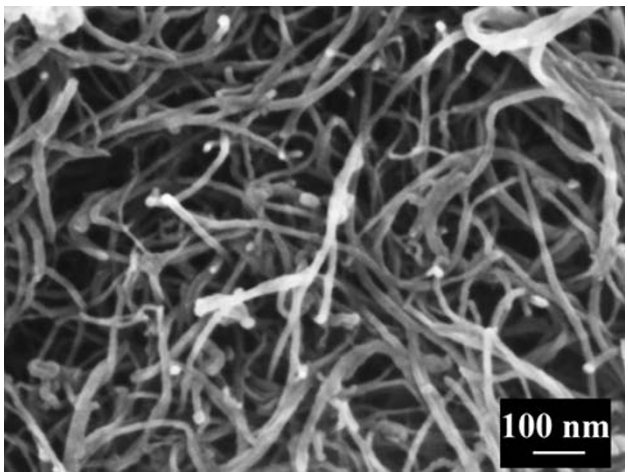

Fig. 5 SEM image of a composite manganese dioxide nanofibers—MWCNT material impregnated into a Ni plaque

particles in the range of 0.5–3 µm, which formed a conductive porous matrix. It was suggested that high surface area, small particle size, porosity and conductivity of Ni plaques are beneficial for application in ES. The SEM image of the impregnated material showed porous fibrous microstructure (Fig. 5) containing manganese dioxide nanofibers and MWCNT.

In the previous investigation [14], it was found that manganese dioxide nanofibers and MWCNT formed a porous fibrous network, which was beneficial for the electrolyte access to the active material. However, the SC of the films deposited on metal foil substrates decreased significantly with increasing film mass from 50 to 300 µg cm^{-2}. In contrast, the results presented below showed that relatively high SC can be obtained for active material loading of 7–15 mg cm^{-2} using Ni plaque current collectors. In this approach, porous Ni current collectors [2] provided improved contact with active material, whereas MWCNT was used as a conductive additive.

Figure 6 shows typical CVs for the composite electrode with material loading of 7 mg cm^{-2}. Within the potential range of 0–1.0 V versus SCE, the composite electrode exhibited capacitive-like current-potential responses, indicated by the box shape of the CVs. It is clear from the Fig. 6 that there are no redox peaks in the range between 0 and 1.0 V. Figure 7 shows SC at different scan rates for the composite electrodes. The SC decreased with increasing scan rate due to the diffusion limitations in pores. The electrodes prepared using powders stirred during 1 h showed higher SC compared to the powders stirred during 20 h. This can be attributed to low agglomeration of the powders stirred during 1 h. This result indicated that further optimization of the powder processing conditions can be beneficial for the improvement in electrode performance. The highest SC of 185 F g^{-1} was achieved at a

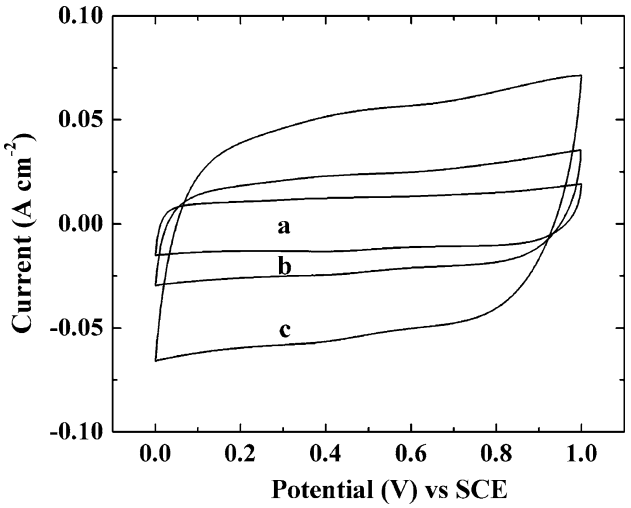

Fig. 6 CVs for a composite electrode containing manganese dioxide nanofibers stirred during 1 h, mixed with MWCNT and impregnated into a Ni plaque with material loading of 7 mg cm^{-2} at scan rates of **a** 10, **b** 20 and **c** 50 mV s^{-1}

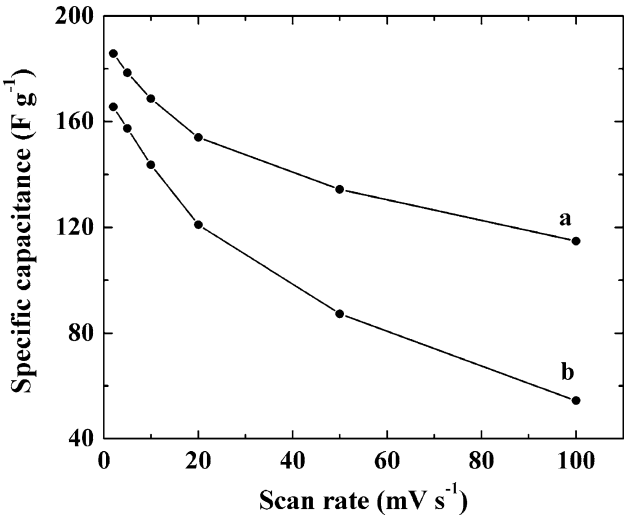

Fig. 8 SC versus scan rate for composite electrodes containing manganese dioxide nanofibers stirred during 1 h, mixed with MWCNT and impregnated into Ni plaques with material loading of **a** 7 mg cm^{-2} and **b** 14 mg cm^{-2}

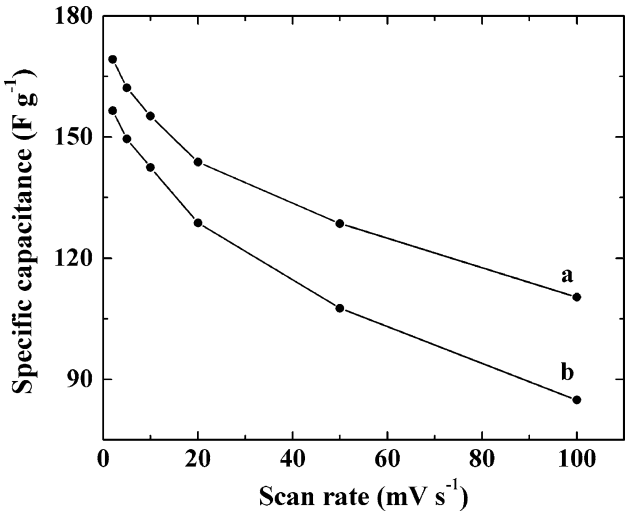

Fig. 7 SC versus scan rate for composite electrode containing manganese dioxide nanofibers stirred during **a** 1 h and **b** 20 h, mixed with MWCNT and impregnated into Ni plaques with material loading of 10 mg cm^{-2}

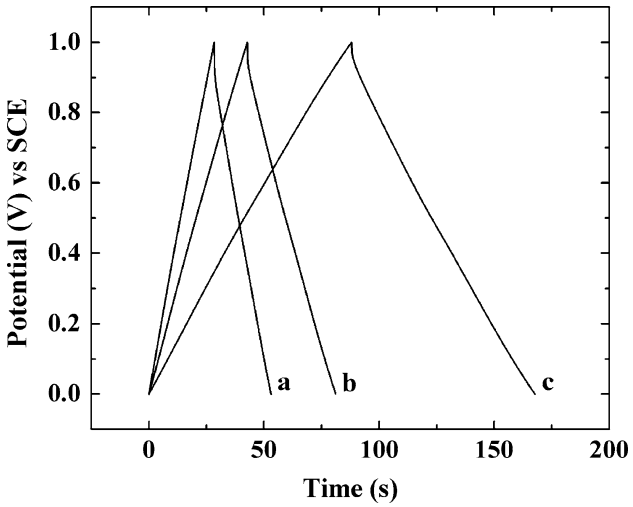

Fig. 9 Charge–discharge behavior for composite electrode containing manganese dioxide nanofibers stirred during 1 h, mixed with MWCNT and impregnated into Ni plaques with material loading of 10 mg cm^{-2} at current densities of **a** 60 **b** 40 and **c** 20 mA cm^{-2}

scan rate of 2 mV s^{-1} for material loading of 7 mg cm^{-2}. However, the SC decreased with increasing material loading (Fig. 8). The reduction in the SC is especially evident at a scan rate of 100 mV s^{-1}. Turning again to the results of the previous investigation [14], it is seen that due to the use of Ni plaque current collectors, the material loading can be increased by 1–2 orders of magnitude, and relatively high SC can be obtained. Moreover, the SC (Fig. 8) at a scan rate of 100 mV s^{-1} for the 7 mg cm^{-2} loading of Ni plaque (SC = 111 F g^{-1}) was higher compared to the SC of the 0.24 mg cm^{-2} film (SC = 82 F g^{-1}) deposited on a foil substrate [14]. The high SC at high scan rates is important for the fabrication of efficient ES [6].

Figure 9 shows charge–discharge behaviour for the composite electrode with material loading of 10 mg cm^{-2}. The charge–discharge curves obtained at different current densities were nearly linear and indicated good capacitive behavior in agreement with box shape CVs shown in Fig. 6. Figure 10 shows impedance spectroscopy data for the sample of the same mass. The equivalent circuit of ES was discussed in the literature and included RC transmission line, describing the porous electrode [5]. C_n elements

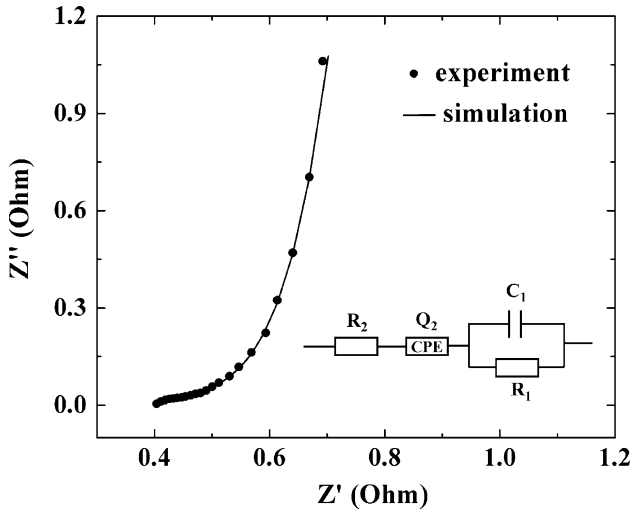

Fig. 10 Impedance spectroscopy data for composite electrode containing manganese dioxide nanofibers stirred during 1 h, mixed with MWCNT and impregnated into Ni plaques with material loading of 10 mg cm^{-2}

represent double-layer capacitance and pseudo capacitance, whereas R_n elements represent electrolyte resistance in pores, Faradaic resistance and equivalent series resistance of the electrodes [18]. Conway and Pell described the impedance of porous electrode using 5-element ($n = 5$) circuit [5]. A constant phase impedance (CPE) element, rather than a pure capacitance C, was used in another investigation [19]. The CPE element describes a 'leaking' capacitor with microscopic roughness of the surface and capacitance dispersion of interfacial origin. The equivalent circuits should allow an optimum representation of the measured spectra with a minimum set of model parameters. Good agreement of simulated and measured data (Fig. 10) was found for the equivalent circuit similar to that proposed for composite ruthenium oxide-graphite electrodes [20]. In this circuit, C_1 and R_1 described double-layer capacitance and charge transfer resistance, respectively. Q_2 described CPE impedance of porous electrode, and R_2 represented electrolyte resistance. The high frequency Z' value of the complex impedance $Z = Z' - iZ''$ showed that $R = R_1 + R_2$ is about 0.4 Ohm for the sample with an area of 1 cm^2. Relatively low resistance R is beneficial for high power ES [18].

Conclusions

Manganese dioxide nanofibers with length ranged from 0.1 to 1 μm and a diameter of about 4–6 nm were prepared by a chemical precipitation method. Composite electrodes for ES, containing two different fibrous materials, were fabricated by impregnation of slurries of the manganese dioxide nanofibers and MWCNT, as a conductive additive, into porous Ni plaque current collectors. The composite electrodes with total mass loading of 7–15 mg cm^{-2} showed good capacitive behavior in the 0.5 M Na_2SO_4 solutions. The reduction in stirring time of the precipitated nanofibers resulted in lower agglomeration and higher SC. The highest SC of 185 F g^{-1} was obtained at a scan rate of 2 mV s^{-1} for materials loading of 7 mg cm^{-2}. Testing results indicated that Ni plaques are promising current collector materials for application in ES.

Acknowledgments The authors gratefully acknowledge the financial support of the Natural Sciences and Engineering Research Council of Canada.

Open Access This article is distributed under the terms of the Creative Commons Attribution Noncommercial License which permits any noncommercial use, distribution, and reproduction in any medium, provided the original author(s) and source are credited.

References

1. V.I. Chani, Q. Yang, D.S. Wilkinson, G.C. Weatherly, J Power Sources **142**, 370 (2005)
2. Q.M. Yang, V.A. Ettel, J. Babjak, D.K. Charles, M.A. Mosoiu, J. Electrochem. Soc. **150**, A543 (2003)
3. E. Cormier, E.B. Wasmund, L.V. Renny, Q.M. Yang, D. Charles, J Power Sources **171**, 999 (2007)
4. A.Y. Zaitsev, D.S. Wilkinson, G.C. Weatherly, T.F. Stephenson, J Power Sources **123**, 253 (2003)
5. B.E. Conway, W.G. Pell, J Power Sources **105**, 169 (2002)
6. P. Simon, Y. Gogotsi, Nat. Mater. **7**, 845 (2008)
7. Y.U. Jeong, A. Manthiram, J. Electrochem. Soc. **149**, A1419 (2002)
8. T. Brousse, M. Toupin, D. Belanger, J. Electrochem. Soc. **151**, 614 (2004)
9. L. Athouel, F. Moser, R. Dugas, O. Crosnier, D. Belanger, T. Brousse, J. Phys. Chem. C **112**, 7270 (2008)
10. S. Devaraj, N. Munichandraiah, Electrochem. Solid-State Lett. **8**, A373 (2005)
11. T. Brousse, P.-L. Taberna, O. Crosnier, R. Dugas, P. Guillemet, Y. Scudeller, Y. Zhou, F. Favier, D. Bélanger, P. Simon, J Power Sources **173**, 633 (2007)
12. S.-C. Pang, M.A. Anderson, T.W. Chapman, J. Electrochem. Soc. **147**, 444 (2000)
13. J.-K. Chang, S.-H. Hsu, W.-T. Tsai, I.W. Sun, J Power Sources **177**, 676 (2008)
14. J. Li, I. Zhitomirsky, J. Mater. Process. Technol. **209**, 3452 (2009)
15. I. Zhitomirsky, L. Gal-Or, J. Mater. Sci. Mater. Med. **8**, 213 (1997)
16. S. Ching, D.J. Petrovay, M.L. Jorgensen, S.L. Suib, Inorg. Chem. **36**, 883 (1997)
17. N. Nagarajan, M. Cheong, I. Zhitomirsky, Mater. Chem. Phys. **103**, 47 (2007)
18. R. Kötz, M. Carlen, Electrochim. Acta **45**, 2483 (2000)
19. W.G. Pell, A. Zolfaghari, B.E. Conway, J. Electroanal. Chem. **532**, 13 (2002)
20. S. Mitra, K.S. Lokesh, S. Sampath, J Power Sources **185**, 1544 (2008)